HHS Public Access

Author manuscript

Eur J Med Chem. Author manuscript; available in PMC 2019 January 01.

Published in final edited form as:

Eur J Med Chem. 2018 January 01; 143: 881–890. doi:10.1016/j.ejmech.2017.12.014.

Structure-guided Design, Synthesis and Evaluation of Oxazolidinone-based Inhibitors of Norovirus 3CL Protease

Vishnu C. Damalanka[a], **Yunjeong Kim**[b], **Anushka C. Galasiti Kankanamalage**[a], **Athri D. Rathnayake**[a], **Nurjahan Mehzabeen**[c], **Kevin P. Battaile**[d], **Scott Lovell**[c], **Harry Nhat Nguyen**[a], **Gerald H. Lushington**[e], **Kyeong-Ok Chang**[b,**], and **William C. Groutas**[a,*]

[a]Department of Chemistry, Wichita State University, Wichita, Kansas 67260, USA

[b]Department of Diagnostic Medicine & Pathobiology, College of Veterinary Medicine, Kansas State University, Manhattan, Kansas 66506, USA

[c]Protein Structure Laboratory, The University of Kansas, Lawrence, Kansas 66047, USA

[d]IMCA-CAT, Hauptman-Woodward Medical Research Institute, APS Argonne National Laboratory, Argonne, IL 60439, USA

[e]LiS Consulting, Lawrence, KS 66046, USA

Abstract

Acute nonbacterial gastroenteritis caused by noroviruses constitutes a global public health concern and a significant economic burden. There are currently no small molecule therapeutics or vaccines for the treatment of norovirus infections. A structure-guided approach was utilized in the design of a series of inhibitors of norovirus 3CL protease that embody an oxazolidinone ring as a novel design element for attaining optimal binding interactions. Low micromolar cell-permeable inhibitors that display anti-norovirus activity have been identified. The mechanism of action, mode of binding, and structural rearrangements associated with the interaction of the inhibitors and the enzyme were elucidated using X-ray crystallography.

Graphical Abstract

*Authors to whom correspondence should be addressed. Department of Chemistry, Wichita State University, Wichita, KS 67260 Tel. (316) 978 7374; Fax: (316) 978 3431, bill.groutas@wichita.edu. **Department of Diagnostic Medicine & Pathobiology, Manhattan, KS 66506 Tel. (785) 532 3849; Fax: (785) 532 4039, kchang@vet.ksu.edu.

Accession codes

Coordinates and structure factors were deposited to the Worldwide Protein Data Bank (wwPDB) with the accession code: 5WEJ

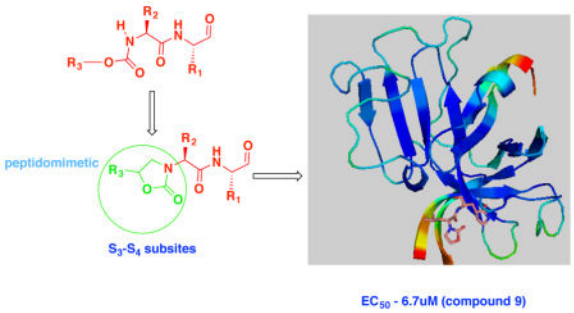

1. Introduction

Human noroviruses are the primary causative agents of acute gastroenteritis and have an increasing impact on public health worldwide [1–3]. While the illness is mild and self-limiting in healthy individuals, it impacts disproportionately and most severely immunocompromised individuals, and the young and elderly [4]. There are 19–21 million norovirus (NV) infections annually in the U.S., and these are associated with high morbidity [5–7]. The toll exacted by NV infections among children <5 years old in developing countries is more acute, resulting in an estimated 71000 deaths annually [8]. The problem is further exacerbated by the highly infectious nature of noroviruses, their genetic diversity and copious virus shedding, as well as their high environmental stability.

Despite the global burden of noroviruses, there are currently no therapeutics or vaccines for the treatment of the disease [9–14], however, recent advances in norovirus pathobiology [15–17], including the identification of proteinaceous receptors for murine norovirus entry into cells [18–19], the nuanced interplay of norovirus pathogenesis and the gut microbiome [20–21], and the development of new in vitro culture systems [22] and animal models [23], have greatly illuminated our understanding of norovirus binding and entry, as well as cell tropism, and have begun to lay a solid foundation for exploring an array of conceptually-sound approaches toward the development of anti-norovirus therapeutics.

Human noroviruses are single-stranded, positive sense RNA viruses belonging to the family *Caliciviridae* [24]. Of the seven genogroups (GI-GVII) in the genus *Norovirus,* genogroups I, II and IV are known to infect humans. The norovirus genome (7–8 kb) consists of three opening reading frames that encode a 200 kDa polyprotein (ORF1), a major capsid protein VP1 (ORF2), and a small basic protein VP2 (ORF3) [25–26]. Co- and post-translational processing of the mature polyprotein precursor by the virus-encoded 3CL protease (NV 3CLpro) generates six mature non-structural proteins.

Norovirus 3CL protease (NV 3CLpro) plays a pivotal role in the life cycle of norovirus through the cleavage of the viral polyprotein and is essential for viral replication. NV 3CL pro is therefore an attractive target for the development of norovirus therapeutics. NV 3CLpro is a chymotrypsin-like cysteine protease with an active site comprised of a prototypical catalytic triad (Cys139-His30-Glu54). The protease functions as an induced fit enzyme and has an extended binding cleft [27–29]. The substrate specificity of the protease

is for a P_1 Gln [30] residue (or Gln surrogate) that engages in critical H-bonding interactions with Thr134 and His157 located in close proximity to the active site.

2. Results and Discussion

2.1 Inhibitor design rationale

NV 3CLpro has been the focus of exploratory investigations by us [31–36] and others [29, 37] as a potential druggable target for the development of anti-norovirus small molecule drugs. Inhibitors of NV 3CLpro reported by us include peptidyl and macrocyclic transition state (TS) inhibitors and TS mimics shown to be effective in enzyme and cell-based assays, as well as efficacious in the mouse model of murine norovirus infection [31]. Reduction of the peptidyl character of an inhibitor typically enhances proteolytic stability, cellular permeability, and oral bioavailability. Depeptidization of an inhibitor can be accomplished via the construction of a macrocyclic inhibitor or a peptidomimetic capable of orienting recognition elements in a specific vector relationship, thereby exploiting binding interactions with active site residues. We hypothesized that the transformation of a peptidyl inhibitor to peptidomimetic (I) (Figure 1) can be accomplished using a functionalized heterocyclic ring (an oxazolidinone). The presence of a ring chiral center was furthermore anticipated to provide directional control for optimal interactions between the S_3-S_4 subsites and recognition element R_3. Since previous studies [31] showed that NV 3CLpro has a strong preference for a cyclohexylalanine (Cha) or Leu as the P_2 residue and a Gln or Gln surrogate [38] as the P1 residue, these recognition elements were incorporated in the structure of inhibitor (I). The design, synthesis, and evaluation of a series of oxazolidinone-derived inhibitors of NV 3CL protease are described herein.

2.2 Chemistry

Compounds ***2a–c*** were synthesized via the epoxidation of the precursor alkenes with *m*-chloroperbenzoic acid to yield the corresponding epoxide which was then treated with (L) Leu-OCH_3 or (L) Cha-OCH_3 in trifluoroethanol (TFE) to yield compounds ***3a–d*** (Scheme 1). Reaction with carbonyl diimidazole (CDI) in dry THF yielded oxazolidinone derivatives ***4a–d*** which were hydrolyzed with LiOH in aqueous THF to yield the corresponding acids ***5a–d.*** Compounds ***5a–d*** were coupled with a glutamine surrogate [38] using EDCI/HOBt/DIEA/DMF to yield compounds ***6a–d*** which, upon reduction with lithium borohydride, generated the corresponding alcohols ***7a–d.*** Oxidation of the alcohols using Dess-Martin periodinane yielded aldehydes ***8–11.*** The corresponding bisulfite adducts ***12–15*** were readily prepared by treating the precursor aldehydes ***8–11*** with $NaHSO_3$/EtOAc/EtOH/H_2O. The final compounds are listed in Table 1.

2.3 Biochemical studies

The inhibitory activity of the synthesized compounds against NV 3CLpro and their anti-norovirus activity in a cell-based replicon system were evaluated as described in the experimental section and the IC_{50}, EC_{50}, and CC_{50} values, are listed in Table 1. These are the average of at least two determinations.

Inspection of the results shown in Table 1 reveals that oxazolidinone derivatives are permeable and, furthermore, some of them display single digit potency (Table 1, compounds ***9***, ***13***, ***10***, and ***14***). Considering that these compounds were screened as mixtures of diastereomers, a further gain in potency may be realized by separating and screening the individual diastereomers. Compounds with a P_2 Cha were about 2-fold more potent than those with a P_2 Leu, confirming previous findings [31]. The position of the phenyl ring, and by extension of the ring substituent, which are probably accommodated in the S_4 subsite of the enzyme, appear to impact potency moderately (*vide infra*).

The mechanism of action and mode of binding of these compounds to the active site of NV 3CLpro were elucidated by determining a high-resolution X-ray crystal structure of inhibitor ***8B*** bound to the enzyme. Examination of the active site revealed the presence of prominent difference electron density consistent with inhibitor ***8B*** covalently bound to Cys 139 (Figure 2A). However, the *m*-chlorobenzyl group of the inhibitor (Figure 2B) was disordered and could not be modeled. The hydrogen bond interactions between NV 3CLpro and ***8B*** are shown in Figure 3A. The expected H-bonds between the -lactam ring of the Gln surrogate with His157 and Thr134 are clearly evident. Furthermore, the backbone hydrogen bonds with Ala158 and Ala160 which serve to correctly position the inhibitor in relation to the catalytic residues and facilitate the reaction of Cys139 with the aldehyde warhead, are also evident. The negatively-charged oxygen of the tetrahedral adduct is stabilized by a hydrogen bond with His30. Dipeptidyl aldehyde inhibitors lacking an oxazolidinone ring form an additional backbone H-bond with Gln110, which is not possible with the oxazolidinone inhibitors (since the oxazolidinone ring N lacks a hydrogen) [31]. Comparison of a previously determined inhibitor bound NV 3CLpro structure of the same crystal form (5T6D) [39] revealed a high degree of similarity with an RMSD deviation of 0.71 Å (154 residues) between Cα atoms using GESAMT (Figure 3B) [40]. However, significant differences are observed in β-strands bII and cII (Gly 92 to Leu 121) which contain Gln 110. The binding of ***8B*** results in the displacement of Gln 110 by 6.89 Å relative to the 5T6D structure (Figure 4). As noted above, the *m*-chlorobenzyl group of ***8B*** was disordered and could not be modeled, however, modeling this portion of the inhibitor in an idealized position would result in a steric clash with Gln 110 (Figure 5). It is surmised that this results in the observed conformational change in the bII and cII strands. It is, however, unclear how the conformational changes induced by the oxazolidinone ring of inhibitor ***8B*** impact potency since inhibitor ***8B*** forms the same number of hydrogen bonds as acyclic inhibitor 5T6D (Figure 3A–B). A likely explanation for this is that the active site conformational changes induced by inhibitor ***8B*** result in sub-optimal positioning of the inhibitor warhead for reaction with the active site Cys139.

3. Conclusion

There is currently a pressing need for the development of norovirus-specific therapeutics and prophylactics for the management of norovirus infections. The studies described herein disclose the structure-based design of the first series of oxazolidinone-based peptidomimetic inhibitors of norovirus 3CL protease. Insights gained from these studies have laid a solid foundation for conducting further optimization of potency and PK characteristics.

4. Experimental section

4.1 General

Reagents and dry solvents were purchased from various chemical suppliers (Aldrich, Oakwood chemicals, Acros Organics, Chem Impex, TCI America, Bachem, and Fisher) and were used as obtained. Silica gel (230–450 mesh) used for flash chromatography was purchased from Sorbent Technologies (Atlanta, GA). Thin layer chromatography was performed using Analtech silica gel plates. The ^{1}H spectra were recorded in $CDCl_3$ or DMSO-d_6 on a Varian XL-400 NMR spectrometer. High resolution mass spectra (HRMS) were performed at the University of Kansas Mass Spectrometry lab using an LCT Premier mass spectrometer (Waters, Milford, MA) equipped with a time of flight mass analyzer and an electrospray ion source or a G6230B TOF MS (Agilent Technologies, Santa Clara, CA). Visualization was accomplished using UV light and/or iodine. All final compounds were purified to ≥95% purity as assessed by HPLC and fully characterized by ^{1}H NMR and HRMS.

4.1.1. Synthesis of compound 1 a–b. General procedure—To a solution of alcohol (35 mmol) in anhydrous DMF (45 mL) was added sodium hydride (1.09 g; 45.5 mmol) portionwise and the reaction mixture was stirred for 15 min at room temperature, followed by the addition of allyl bromide (4.23 g; 35 mmol) and stirring the reaction mixture overnight at room temperature. The solvent was removed *in vacuo* and the residue was partitioned between ethyl acetate (150 mL) and 5% aqueous HCl (2 × 50 mL). The layers were separated and the organic layer was washed with saturated aqueous $NaHCO_3$ (2 × 50 mL), followed by saturated NaCl (50 mL). The organic layer was dried over anhydrous Na_2SO_4, filtered, and concentrated to yield an oily product.

4.1.1.1. 1-(allyloxy)-3-chlorobenzene 1a: Oil (yield 83%); ^{1}H NMR (400 MHz, $CDCl_3$) δ ppm 4.58–4.62 (d, J = 11.02, 2H), 5.46-5.31 (m, 2 H), 6.18-6.04 (m, 1 H), 7.35-7.03 (m, 4H). HRMS (ESI) calcd for $C_9H_{10}ClO$: $[M+H]^+$: 169.0420 Found 169.0437.

4.1.1.2. 1-[(allyloxy)methyl]-3-chlorobenzene 1b: Oil (yield 84%); ^{1}H NMR (400 MHz, $CDCl_3$) δ ppm 4.10-4.02 (d, J = 10.12, 2H), 4.78-4.73 (s, 2H), 5.38-5.28 (m, 2 H), 6.10-6.05 (m, 1 H), 7.40-7.12 (m, 4H). HRMS (ESI) calcd for $C_{10}H_{12}ClO$: $[M+H]^+$: 183.0577 Found 183.0595.

4.1.2. Synthesis of compounds 2a–c. General procedure—To a solution of the appropriate alkene (35 mmol) in dry DCM (100 mL) was added *m*-CPBA (42 mmol) at 0°C. The ice bath was removed and the reaction mixture was stirred at room temperature overnight (18 h). The consumption of starting material was monitored by TLC. The reaction mixture was cooled to 0 – 5°C and quenched with aqueous 1N NaOH solution (15 mL). The reaction mixture was partitioned between water (100 mL) and DCM (100 mL) and the layers were separated. The aqueous layer was extracted with DCM (100 mL) and the combined organic layers were washed with brine (50 mL). The organic layer was dried over anhydrous Na_2SO_4, filtered and concentrated to yield an oily product.

4.1.2.1. 2-(3-chlorobenzyl)oxirane 2a: Oil (yield (88%); ^{1}H NMR (400 MHz, $CDCl_3$) δ ppm 2.54 (dd, *J* = 4.93, 2.62 Hz, 1H), 2.87-2.72 (m, 1H), 3.36 (d, *J* = 6.77 Hz, 1H), 3.16-3.07 (m, 2H), 7.67-7.03 (m, 4H). HRMS (ESI) calcd for $C_9H_{10}ClO$: $[M+H]^+$: 169.0420 Found 169.0427.

4.1.2.2. 2-[(3-chlorophenoxy) methyl] oxirane 2b: Oil (yield 85%); ^{1}H NMR (400 MHz, $CDCl_3$) δ ppm 2.75 (dd, *J* = 4.90, 2.64 Hz, 1H), 3.00-2.89 (m, 1H), 3.35 (tdd, *J* = 5.70, 4.10, 2.86, 2.86 Hz, 1H), 3.93 (dd, *J* = 11.02, 5.73 Hz, 1H), 4.22 (dd, *J* = 11.02, 3.04 Hz, 1H), 7.35-7.03 (m, 4H). HRMS (ESI) calcd for $C_9H_{10}ClO_2$: $[M+H]^+$: 185.0369 Found 185.0377.

4.1.2.3. 2-{[(3-chlorobenzyl) oxy] methyl} oxirane 2c: Oil (yield 84%); ^{1}H NMR (400 MHz, $CDCl_3$) δ ppm 2.61 (dd, *J* = 4.90, 2.64 Hz, 1H), 2.95-2.85 (m, 1H), 3.30 (tdd, *J* = 5.70, 4.10, 2.86, 2.86 Hz, 1H), 3.97 (dd, *J* = 11.02, 5.73 Hz, 1H), 4.25 (dd, *J* = 11.02, 3.04 Hz, 1H), 4.52 (s, 2H), 7.35-7.03 (m, 4H). HRMS (ESI) calcd for $C_{10}H_{12}ClO_2$: $[M+H]^+$: 199.0526 Found 199.0534.

4.1.3. Synthesis of compounds 3a–d. General procedure—To a solution of compound ***2*** (29.65 mmol) in trifluoroethanol (50 mL) was added the corresponding free amino acid ester (29.65 mmol) at room temperature. The reaction mixture was refluxed for 6 h with stirring. The progress of the reaction was monitored by TLC. The reaction mixture was cooled to room temperature and the solvent was removed. The crude residue was purified by flash chromatography to yield a colorless oil.

4.1.3.1. Methyl [3-(3-chlorophenyl)-2-hydroxypropyl]-L-leucinate 3a: Oil (yield 70%); ^{1}H NMR (400 MHz, $CDCl_3$) δ ppm 1.06-0.89 (d, 6H), 1.53-1.49 (m, 1H), 1.77-1.70 (m, 2H), 3.30-2.44 (m, 4H), 3.71 (s, 3H), 4.12 (tt, *J* = 7.15, 7.15, 3.57, 3.57 Hz, 1H), 4.85-4.48 (m, 1H), 5.70—5-60 (br. s, 1H), 7.53-7.01 (m, 4H). HRMS (ESI) calcd for $C_{16}H_{25}ClNO_3$: $[M+H]^+$: 314.1523 Found 314.1532.

4.1.3.2. Methyl (2S)-2-{[3-(3-chlorophenyl)-2-hydroxypropyl] amino}-3-cyclohexylpropanoate 3b: Oil (yield 75%); ^{1}H NMR (400 MHz, $CDCl_3$) δ ppm 1.93-0.76 (m, 13H), 2.71 (m, 4H), 3.52-3.47 (m, 1H), 3.70-3.60 (s, 3H), 3.95 (m, 1H), 5.18-5.04 (m, 1H), 7.49-7.03 (m, 4H). HRMS (ESI) calcd for $C_{19}H_{29}ClNO_3$: $[M+H]^+$: 354.1836 Found 354.1845.

4.1.3.3. Methyl [3-(3-chlorophenoxy)-2-hydroxypropyl]-L-leucinate 3c: Oil (yield 72%); ^{1}H NMR (400 MHz, $CDCl_3$) δ ppm 0.96-0.89 (d, 6H), 1.52-1.49 (m, 1H), 1.78-1.72 (m, 2H), 2.84-2.61 (m, 3H), 3.68 (s, 3H), 4.24-3.98 (m, 3H), 4.85-4.78 (m, 1H), 5.70—5-60 (br. s, 1H), 7.53-7.01 (m, 4H). HRMS (ESI) calcd for $C_{16}H_{25}ClNO_4$: $[M+H]^+$: 330.1472 Found 330.1523.

4.1.3.4. Methyl {3-[(3-chlorobenzyl) oxy]-2-hydroxypropyl}-L-leucinate 3d: Oil (yield 71%); ^{1}H NMR (400 MHz, $CDCl_3$) δ ppm 0.99-0.87 (d, 6H), 1.55-1.48 (m, 1H), 1.77-1.73 (m, 2H), 2.77-2.54 (m, 3H), 3.62-3.73 (m, 3 H), 3.71 (s, 3H), 4.64 (s, 2H), 5.25-5.18 (br. s, 1H), 5.70—5-60 (br. s, 1H), 7.53-7.01 (m, 4H). HRMS (ESI) calcd for $C_{19}H_{27}ClNO_4$: $[M+H]^+$: 344.1629 Found 344.1639.

4.1.4. Synthesis of compounds 4a–d. General procedure—To a solution of compound ***3*** (21 mmol) in anhydrous THF (75 mL) kept at room temperature was added carbonyl diimidazole (42 mmol) and the reaction mixture was refluxed for 5 h. The disappearance of the starting material was monitored by TLC. The reaction mixture was cooled to room temperature and the solvent was removed in vacuo. The residue was partitioned between EtOAc (250 mL) and 5% aq HCl (100 mL). The layers were separated and the organic layer was sequentially washed with 5% aq HCl, saturated $NaHCO_3$ (2×100 mL) and brine (100 mL). The organic layer was dried over anhydrous Na_2SO_4, filtered and concentrated to yield a crude product which was purified by flash chromatography.

4.1.4.1. Methyl (2S)-2-[5-(3-chlorobenzyl)-2-oxooxazolidin-3-yl]-4-methylpentanoate 4a: Oil (yield 45%); ^{1}H NMR (400 MHz, $CDCl_3$) δ ppm 7.38-7.06 (m, 4H), 0.98-0.79 (d, 6H), 1.85-1.53 (m, 3H), 3.15-2.81 (m, 2H), 3.50-3.30 (m, 2H), 3.72 (s, 3H), 4.60-4.50 (m, 1H), 4.82-4.75 (m, 1H). HRMS (ESI) calcd for $C_{17}H_{23}ClNO_4$: $[M+H]^+$: 340.1316 Found 340.1321.

4.1.4.2. Methyl (2S)-2-[5-(3-chlorobenzyl)-2-oxooxazolidin-3-yl]-3-cyclohexylpropanoate 4b: Oil (yield 45%); ^{1}H NMR (400 MHz, $CDCl_3$) δ ppm 1.90-0.74 (m, 13H), 3.09-2.84 (m, 2H), 3.82-3.63 (m, 2H), 4.85-4.55 (m, 2H), 7.37-7.05 (m, 4H). HRMS (ESI) calcd for $C_{20}H_{27}ClNO_4$: $[M+H]^+$: 380.1629 Found 380.1642.

4.1.4.3. Methyl(2S)-2-{5-[(3-chlorophenoxy) methyl]-2-oxooxazolidin-3-yl}-4-methylpentanoate 4c: Oil (yield 44%); ^{1}H NMR (400 MHz, $CDCl_3$) δ ppm 1.03-0.86 (d, 6H), 1.85-1.78 (m, 1H), 1.50-1.47 (m, 1H), 3.05-2.88 (m, 4H), 3.76 (s, 3H), 3.80-3.70 (m, 1H), 4.60-4.50 (m, 1H), 7.45-7.14 (m, 4H). HRMS (ESI) calcd for $C_{17}H_{23}ClNO_5$: $[M+H]^+$: 356.1265 Found 356.1284.

4.1.4.4. Methyl(2S)-2-(5-{[(3-chlorobenzyl) oxy] methyl}-2-oxooxazolidin-3-yl)-4-methylpentanoate 4d: Oil (yield 40%); ^{1}H NMR (400 MHz, $CDCl_3$) δ ppm 1.05-0.76 (d, 6H), 1.87-1.77 (m, 1H), 1.50 (m, 1H), 2.95-2.85 (m, 4H), 3.73 (s, 3H), 3.77-3.60 (m, 1H), 4.59-4.50 (m, 1H), 4.76-4.68 (s, 3H), 7.42-7.16 (m, 4H). HRMS (ESI) calcd for $C_{18}H_{25}ClNO_5$: $[M+H]^+$: 370.1421 Found 370.1437.

4.1.5. Synthesis of compounds 5a–d. General procedure—A solution of ester ***4*** (9 mmol) in tetrahydrofuran (25 mL) was treated with 1M aqueous LiOH (25 mL). The reaction mixture was stirred for 3 h at room temperature while monitoring the disappearance of the ester by TLC. Most of the solvent was evaporated off and the solution was acidified to pH ~3 using 5% hydrochloric acid (10 mL). The aqueous layer was extracted with ethyl acetate (2 × 100 mL) and the combined organic layers were washed with brine (50 mL). The organic layer was dried over anhydrous sodium sulfate, filtered, and concentrated to yield compound ***5.***

4.1.5.1. (2S)-2-[5-(3-chlorobenzyl)-2-oxooxazolidin-3-yl]-4-methylpentanoic acid 5a: White solid (yield 93%); mp 129–130°C, ^{1}H NMR (400 MHz, $CDCl_3$) δ ppm 7.57-6.98 (m, 4H), 5.06-4.67 (m, 1H), 4.77-4.42 (m, 1H), 3.34-2.72 (m, 3H), 3.48 (d, J = 7.94 Hz, 1H),

1.96-1.37 (m, 5H), 1.05-0.83 (d, 6H). HRMS (ESI) calcd for $C_{16}H_{20}ClNNaO_4$: $[M+Na]^+$: 348.0979 Found 348.0995.

4.1.5.2. (2S)-2-[5-(3-chlorobenzyl)-2-oxooxazolidin-3-yl]-3-cyclohexylpropanoic acid 5b: Viscous oil (yield 94%); ^{1}H NMR (400 MHz, $CDCl_3$) δ ppm 1.03-0.74 (m, 6H), 1.26 (t, *J* = 7.16, 7.16 Hz, 2H), 1.85-1.39 (m, 5H), 2.50-2.25 (m, 2H), 3.00-2.75 (m, 2H), 3.80-3.65 (m, 1H), 4.54-4.39 (m, 1H), 4.87-4.76 (m, 1H), 7.38-7.01 (m, 4H). HRMS (ESI) calcd for $C_{19}H_{25}ClNNaO_4$: $[M+Na]^+$: 388.1292 Found 388.1309.

4.1.5.3. 2-{5-[(3-chlorophenoxy) methyl]-2-oxooxazolidin-3-yl}-4-methylpentanoic acid 5c: Viscous oil (yield 95%); ^{1}H NMR (400 MHz, $CDCl_3$) δ ppm 1.03-0.86 (d, 6H), 1.85-1.78 (m, 1H), 1.50-1.47 (m, 1H), 3.05-2.88 (m, 4H), 3.80-3.70 (m, 1H), 4.60-4.50 (m, 1H), 7.45-7.14 (m, 4H). HRMS (ESI) calcd for $C_{16}H_{21}ClNO_5$: $[M+H]^+$: 342.1108 Found 342.1125.

4.1.5.4. 2-(5-{[(3-chlorobenzyl) oxy] methyl}-2-oxooxazolidin-3-yl)-4-methylpentanoic acid 5d: Viscous oil, yield (95%), ^{1}H NMR (400 MHz, $CDCl_3$) δ ppm 1.05-0.76 (d, 6H), 1.87-1.77 (m, 1H), 1.50 (m, 1H), 2.95-2.85 (m, 4H), 3.77-3.60 (m, 1H), 4.59-4.50 (m, 1H), 4.76-4.68 (s, 3H), 7.42-7.16 (m, 4H). HRMS (ESI) calcd for $C_{17}H_{23}ClNO_5$: $[M+H]^+$: 356.1265 Found 356.1278.

4.1.6. Synthesis of compounds 6a–d. General procedure—To a solution of ***5*** (8.2 mmol) in dry DMF (20 mL) was added EDCI (10.6 mmol, 1.3 eq.) and HOBt (10.6 mmol, 1.3 eq) and the mixture was stirred for 30 minutes at room temperature. In a separate flask, a solution of boc-deprotected glutamine surrogate (8.2 mmol) in dry DMF (20 mL) cooled to 0–5°C was treated with diisopropylethylamine (32.8 mmol, 4.0 eq) and the solution was stirred for 30 minutes. It was then added to the solution above and the reaction mixture was stirred for 16 h while monitoring the reaction by TLC. The solvent was removed *in vacuo* and the residue was partitioned between ethyl acetate (200 mL) and 10% citric acid (75 mL). The layers were separated and the organic layer was washed with saturated aqueous $NaHCO_3$ (2 × 75 mL), followed by saturated NaCl (75 mL). The organic layer was dried over anhydrous Na_2SO_4, filtered, and concentrated. The crude residue was purified by flash chromatography to yield the product as a white solid.

4.1.6.1. Methyl (2S)-2-{(2S)-2-[5-(3-chlorobenzyl)-2-oxooxazolidin-3-yl]-4-methylpentanamido}-3-[(S)-2-oxopyrrolidin-3-yl] propanoate 6a: diastereomers A and B were separated using flash chromatography. **(A)** White solid (yield 32%); mp 47–48°C, ^{1}H NMR (400 MHz, $CDCl_3$) δ ppm 0.93 (ddd, *J* = 25.59, 17.70, 6.33 Hz, 6H), 1.63 (td, *J* = 14.14, 7.53, 7.53 Hz, 1H), 1.85 (ddd, *J* = 13.52, 7.86, 2.99 Hz, 2H), 2.37 (m, 4H), 2.89 (dd, *J* = 14.02, 6.52Hz, 1H), 3.12 (dd, *J* = 14.09, 7.06 Hz, 1H), 3.50-3.31 (m, 2H), 3.69-3.50 (m, 4H), 3.77-3.67 (s, 3H), 4.33 (d, *J* = 6.05 Hz, 1H), 4.88-4.54 (m, 1H), 6.63 (d, 1H), 7.49-7.12 (m, 4H), 8.34 (d, *J* = 4.87Hz, 1H). HRMS (ESI) calcd for $C_{24}H_{32}ClN_3NaO_6$: $[M+Na]^+$: 516.1877 Found 516.1981.

(B) White solid (yield 25%); mp 51–52°C, ^{1}H NMR (400 MHz, $CDCl_3$) δ ppm 0.95 (d, *J* = 20.12 Hz, 6H), 1.72-1.66 (td, *J* = 14.14, 7.53, 7.53 Hz, 1H), 1.90-1.83 (dd, *J* = 11.14, 7.12

Hz, 2H), 2.50-2.37 (m, 4H), 2.90-2.79 (dd, *J* = 14.02, 6.52Hz, 1H), 3.26-3.11 (d, 1H), 3.45-3.32 (m, 2H), 3.68-3.52 (m, 4H), 3.72-3.68 (s, 3H), 4.51 (d, *J* = 6.25 Hz, 1H), 4.90-4.85 (m, 1H), 6.83 (d, 1H), 7.51-7.22 (m, 4H), 8.34 (d, *J* = 4.82 Hz, 1H). HRMS (ESI) calcd for $C_{24}H_{32}ClN_3NaO_6$: $[M+Na]^+$: 516.1877 Found 516.1862.

4.1.6.2. Methyl (2S)-2-{(2S)-2-[5-(3-chlorobenzyl)-2-oxooxazolidin-3-yl]-3-cyclohexylpropanamido}-3-[(S)-2-oxopyrrolidin-3-yl] propanoate 6b: White solid (yield 58%); mp 88–89°C, ^{1}H NMR (400 MHz, $CDCl_3$) δ ppm 1.34-0.77 (m, 11H), 1.67 (m, 2H), 3.11-2.66 (m, 4H), 2.68-2.27 (m, 4H), 3.54-3.25 (m, 4H), 3.72 (s, 3H), 5.01-4.36 (m, 2H), 7.43-7.08 (m, 4H), 9.85-9.45 (br. s, 1H). HRMS (ESI) calcd for $C_{27}H_{36}ClN_3NaO_6$: $[M+Na]^+$: 556.2190 Found 556.2204.

4.1.6.3. Methyl (2S)-2-[(2S)-2-{5-[(3-chlorophenoxy) methyl]-2-oxooxazolidin-3-yl}-4-methylpentanamido]-3-{(S)-2-oxopyrrolidin-3-yl} propanoate 6c: White solid (yield 65%); mp 45–46°C,^{1}H NMR (400 MHz, $CDCl_3$) δ ppm 1.08-0.89 (d, 6H), 1.53-1.47 (m, 1H) 1.93-1.71 (m, 2H), 2.51-2.25 (m, 2H), 3.37 (dd, *J* = 6.18, 3.43 Hz, 2H), 3.57 (dd, *J* = 8.95, 6.07 Hz, 2H), 3.79-3.71 (s, 3H), 4.12 (dtd, *J* = 14.73, 10.42, 10.40, 5.24 Hz, 2H), 4.68 (t, *J* = 7.77, 7.77 Hz, 1H), 4.89 (m, 1H), 7.01-6.65 (m, 2H), 7.31-7.12 (m, 2H), 8.44 (d, *J* = 6.05 Hz, 1H). HRMS (ESI) calcd for $C_{24}H_{32}ClN_3NaO_7$: $[M+Na]^+$: 532.1826 Found 532.1730.

4.1.6.4. Methyl (2S)-2-[(2S)-2-(5-{[(3-chlorobenzyl) oxy] methyl}-2-oxooxazolidin-3-yl)-4-methylpentanamido]-3-{(S)-2-oxopyrrolidin-3-yl} propanoate 6d: White solid (yield 68%); mp 47–48°C, ^{1}H NMR (400 MHz, $CDCl_3$) δ ppm 1.04-0.79 (d, 6H), 1.91-1.53 (m, 3H), 2.48-2.13 (m, 4H), 3.42-3.18 (m, 4H), 3.81-3.60 (m, 2H), 3.79-3.71 (s, 3H), 4.12 (d, *J* = 7.14 Hz, 1H), 4.42-4.31 (m, 2H), 4.65-4.49 (s, 2H), 6.36 (br.s, 1H), 7.36-7.13 (m, 4H), 8.15 (d, *J* = 6.48 Hz, 1H). HRMS (ESI) calcd for $C_{25}H_{34}ClN_3NaO_7$: $[M+Na]^+$: 546.1983 Found 546.1894.

4.1.7. Synthesis of compounds 7a–d. General procedure—To a solution of ester (1.87 mmol) in anhydrous THF (10 mL) was added dropwise lithium borohydride (2M in THF, 2.8 mL, 5.61 mmol) followed by anhydrous methanol (10 mL), and the reaction mixture was stirred at room temperature overnight. The reaction mixture was then acidified by adding 5% aqueous HCl until the pH of the solution was ~3. Removal of the solvent left a residue which was taken up in ethyl acetate (100 mL). The organic layer was washed with brine (25 mL), dried over anhydrous sodium sulfate, filtered, and concentrated to yield the desired alcohol.

4.1.7.1. (2S)-2-[5-(3-chlorobenzyl)-2-oxooxazolidin-3-yl]-N-{(S)-1-hydroxy-3-[(S)-2-oxopyrrolidin-3-yl] propan-2-yl}-4-methylpentanamide 7a: (A) White solid (yield 93%); mp 59–60°C, ^{1}H NMR (400 MHz, $CDCl_3$ δ 1.02-0.71 (d, 6H), 2.06-1.38 (m, 4H), 2.67-2.17 (m, 4H), 2.98-2.75 (m, 4H), 3.55-3.05 (m, 4H), 3.74-3.45 (m, 1H), 3.87 (t, *J* = 8.75, 8.75 Hz, 1H), 4.36 (m, 1H), 5.06-4.63 (m, 1H), 6.41-5.91 (d, 1H), 7.51-6.93 (m, 4H), 8.20-7.78 (d, 1H). HRMS (ESI) calcd for $C_{23}H_{32}ClN_3NaO_5$: $[M+Na]^+$: 488.1928 Found 488.1835.

(B) White solid (yield 95%); mp 65–66°C, ^{1}H NMR (400 MHz, $CDCl_3$) δ 0.94-0.85 (d, 6H), 2.36-1.72 (m, 4H), 2.57-2.25 (m, 4H), 3.02-2.85 (m, 4H), 3.60-3.15 (m, 4H), 3.75-3.45 (m, 1H), 3.92-3.88 (t, *J* = 8.68, 8.68 Hz, 1H), 4.52 (m, 1H), 5.12-4.78 (m, 1H), 6.45-6.12 (d, 1H), 7.55-7.03 (m, 4H), 8.01-7.94 (d, 1H). HRMS (ESI) calcd for $C_{23}H_{32}ClN_3NaO_5$: $[M+Na]^+$: 488.1928 Found 488.1835.

4.1.7.2. (2S)-2-[5-(3-chlorobenzyl)-2-oxooxazolidin-3-yl]-3-cyclohexyl-N-{(S)-1-hydroxy-3-[(S)-2-oxopyrrolidin-3-yl] propan-2-yl} propanamide 7b: White solid (yield 94%); mp 133–134°C, ^{1}H NMR (400 MHz, DMSO-d_6) δ ppm 1.20-0.76 (m, 9H), 1.81-1.53 (m, 6H), 2.78-2.68 (m, 4H), 3.42-3.13 (m, 4H), 3.93-3.78 (m, 4H), 4.46-4.26 (m, 1H), 4.95-4.75 (m, 1H), 7.17-7.09 (s, 1H), 7.27-7.14 (m, 3H), 7.97-7.88 (br. s, 1H), 9.80-9.65 (br. s, 1H). HRMS (ESI) calcd for $C_{26}H_{36}ClN_3NaO_5$: $[M+Na]^+$: 528.2241 Found 528.22321.

4.1.7.3. (2S)-2-{5-[(3-chlorophenoxy) methyl]-2-oxooxazolidin-3-yl}-N-[(S)-1-hydroxy-3-{(S)-2-oxopyrrolidin-3-yl} propan-2-yl]-4-methylpentanamide 7c: White solid (yield 93%); mp 58–59°C, ^{1}H NMR (400 MHz, $CDCl_3$ δ 1.03-0.82 (d, 6H), 1.55-1.50 (m, 2H), 2.65-2.22 (m, 6H), 3.30-3.21 (m, 2H), 3.80-3.50 (m, 4H), 4.39-4.05 (m, 2H), 5.02-4.76 (m, 1H), 7.07-6.90 (m, 1H), 7.46-7.13 (m, 3H), 8.21-8.01 (br. s, 1H). HRMS (ESI) calcd for $C_{23}H_{32}ClN_3NaO_6$: $[M+Na]^+$: 504.1877 Found 504.1804.

4.1.7.4. (2S)-2-(5-{[(3-chlorobenzyl) oxy] methyl}-2-oxooxazolidin-3-yl)-N-[(S)-1-hydroxy-3-{(S)-2-oxopyrrolidin-3-yl} propan-2-yl]-4-methylpentanamide 7d: White solid (yield 93%); ^{1}H NMR (400 MHz, $CDCl_3$ δ 1.14-0.79 (d, 6H), 1.50 (dd, *J* = 28.65, 20.93 Hz, 2H), 2.71-2.20 (m, 6H), 3.34 (m, 2H), 3.82-3.45 (m, 4H), 4.36-3.85 (m, 2H), 4.52 (s, 2H), 5.13-4.78 (m, 1H), 7.07-6.70 (m, 1H), 7.40-7.10 (m, 3H), 8.20-7.93 (br. s, 1H). HRMS (ESI) calcd for $C_{24}H_{33}ClN_3O_6$: $[M-H]^+$: 494.2058 Found 494.2402.

Synthesis of aldehydes 8–11. General procedure—A representative alcohol (2.07 mmol) was dissolved in anhydrous dichloromethane (30 mL) under a nitrogen atmosphere and cooled to 0°C. Dess-Martin periodinane (1.75 g, 4.14 mmol, 2.0 eq.) was added to the reaction mixture with stirring. The ice bath was removed and the reaction mixture was stirred at room temperature for 3 h (monitoring by TLC indicated complete disappearance of the starting material). A solution of 40 mM sodium thiosulfate in saturated aqueous $NaHCO_3$ (50 mL) was added and the solution was stirred for another 15 minutes. The aqueous layer was removed and the organic layer was washed with sodium bicarbonate (25 mL), water (2 × 25 mL) and brine (25 mL). The organic layer was dried over anhydrous sodium sulfate, filtered and concentrated. The crude aldehyde was purified by flash chromatography (silica gel/methylene chloride/ethyl acetate/methanol).

(2S)-2-[5-(3-chlorobenzyl)-2-oxooxazolidin-3-yl]-4-methyl-N-[(S)-1-oxo-3-{(S)-2-oxopyrrolidin-3-yl} propan-2-yl] pentanamide (8): (A) White solid, mp 60–61°C, yield (75%), ^{1}H NMR (400 MHz, $CDCl_3$) δ ppm 1.05-0.81 (d, 6H), 1.32-1.27 (m, 1H), 1.75-1.49 (m, 2H), 2.38-2.12 (m, 4H), 2.74-2.54 (m, 4H), 3.21-3.13 (m, 2H), 3.40 (d, *J* = 4.42 Hz, 1H), 3.61 (d, *J* = 39.11 Hz, 1H), 4.29-4.20 (m, 1H), 6.16-5.99 (m, 1H), 7.34-7.09 (m, 4H), 8.55-8.45 (d, 1H), 9.48 (s, 1H), 9.78-9.76 (br. s, 1H). HRMS (ESI) calcd for $C_{23}H_{29}ClN_3O_5$: $[M-H]^+$: 462.1796 Found 462.2080.

(B) White solid, mp 54–55°C, yield (70%), ^{1}H NMR (400 MHz, $CDCl_3$) δ ppm 0.98-0.77 (d, 1H), 1.60 (ddd, *J* = 15.25, 9.74, 5.00 Hz, 1H), 1.84 (ddd, *J* = 6.61, 5.82, 3.56 Hz, 2H), 2.60-2.40 (m, 5H), 2.99 (dd, *J* = 7.47, 5.78 Hz, 2H), 3.20 (dd, *J* = 8.77, 6.54 Hz, 2H), 3.40-3.27 (m, 2H), 3.96-3.66 (m, 1H), 4.29-3.97 (m, 1H), 4.52 (dd, *J* = 10.39, 5.38 Hz, 1H), 6.34 (s, 1H), 7.19-7.09 (m, 1H), 7.39-7.16 (m, 3H), 8.64 (s, 1H), 9.44 (s, 1H). HRMS (ESI) calcd for $C_{23}H_{29}ClN_3O_5$: $[M-H]^+$: 462.1796 Found 462.1825.

(2S)-2-[5-(3-chlorobenzyl)-2-oxooxazolidin-3-yl]-3-cyclohexyl-N-[(S)-1-oxo-3-{(S)-2-oxopyrrolidin-3-yl} propan-2-yl] propanamide (9): White solid, mp 76–77°C, yield (70%),^{1}H NMR (400 MHz, $CDCl_3$) δ ppm 1.15-0.75 (m, 9H), 2.17-1.37 (m, 6H), 2.51-2.31 (m, 2H), 3.09-2.89 (m, 4H), 3.47-3.24 (m, 2H), 3.94-3.67 (m, 2H), 4.27-4.09 (m, 1H), 4.71-4.38 (m, 1H), 5.02-4.71 (m, 1H), 7.37-7.05 (m, 4H), 8.75-8.57 (d, 1H), 9.50-9.46 (s, 1H). HRMS (ESI) calcd for $C_{26}H_{33}ClN_3O_5$: $[M-H]^+$: 502.2109 Found 502.2212.

(2S)-2-{5-[(3-chlorophenoxy) methyl]-2-oxooxazolidin-3-yl}-4-methyl-N-[(S)-1-oxo-3-{(S)-2-oxopyrrolidin-3-yl} propan-2-yl] pentanamide (10): White solid, mp 53–54°C, yield (65%), ^{1}H NMR (400 MHz, $CDCl_3$) δ ppm 1.08-0.89 (d, 6H), 1.53-1.47 (m, 1H) 1.93-1.71 (m, 2H), 2.51-2.25 (m, 2H), 3.37 (dd, *J* = 6.18, 3.43 Hz, 2H), 3.57 (dd, *J* = 8.95, 6.07 Hz, 2H), 3.79-3.71 (s, 3H), 4.12 (dtd, *J* = 14.73, 10.42, 10.40, 5.24 Hz, 2H), 4.68 (t, *J* = 7.77, 7.77 Hz, 1H), 4.89 (m, 1H), 7.01-6.65 (m, 2H), 7.31-7.12 (m, 2H), 8.44 (d, *J* = 6.05 Hz, 1H). HRMS (ESI) calcd for $C_{23}H_{29}ClN_3O_6$: $[M-H]^+$: 478.1745 Found 478.2065.

(2S)-2-(5-{[(3-chlorobenzyl) oxy] methyl}-2-oxooxazolidin-3-yl)-4-methyl-N-[(S)-1-oxo-3-{(S)-2-oxopyrrolidin-3-yl} propan-2-yl] pentanamide (11): White solid, mp 45–46°C, yield (55%), ^{1}H NMR (400 MHz, $CDCl_3$) δ ppm 1.14-0.81 (d, 6H), 1.26 (t, *J* = 7.15, 7.15 Hz, 1H), 1.80 (ddd, *J* = 25.33, 24.66, 17.19 Hz, 2H), 2.41-2.10 (m, 5H), 3.43-3.20 (m, 6H), 4.62-4.43 (m, 2H), 4.70 (s, 2H), 5.70-5.58 (m, 1H), 5.94-5.86 (m, 1H), 7.44-7.11 (m, 4H), 8.35-8.25 (d, 1H), 9.42 (s, 1H). HRMS (ESI) calcd for $C_{24}H_{31}ClN_3O_6$: $[M-H]^+$: 492.1901 Found 492.2206.

Synthesis of aldehyde bisulfite salts 12–15. General procedure—To a solution of aldehyde ***8–11*** (0.20 mmol) in dry ethyl acetate (1.0 mL) was added absolute ethanol (0.5 mL) with stirring, followed by a solution of sodium bisulfite (0.20 mmol) in water (0.20 mL). The reaction mixture was stirred for 3 h at 50 °C, allowed to cool to room temperature, and then vacuum filtered. The solid was thoroughly washed with absolute ethanol and the filtrate was dried over anhydrous sodium sulfate, filtered, and concentrated to yield a yellowish oil. The oily product was treated with ethyl ether (2 × 5 mL) to form a white solid. The white solid was sequentially stirred with ethyl ether (3 mL) and ethyl acetate (1.5 mL) for 5 minutes. Careful removal of the solvent using a pipette left behind the product as a white solid.

Sodium (2S)-2-{(2S)-2-[5-(3-chlorobenzyl)-2-oxooxazolidin-3-yl]-4-methylpentanamido}-1-hydroxy-3-[(S)-2-oxopyrrolidin-3-yl] propane-1-sulfonate (12): (A) White solid, mp 99–100°C, yield (67%),^{1}H NMR (400 MHz, *DMSO-d6*) δ ppm 0.90-0.83 (d, 6H), 1.75-1.32 (m, 4H), 2.28-2.06 (m, 2H), 2.94-2.80 (m, 3H), 3.83-3.67 (m, 4H), 3.99-3.91 (m, 2H), 4.35-3.96 (m, 2H), 4.99-4.73 (m, 2H), 7.35 (d, *J* = 11.88 Hz, 1H), 7.75-7.62 (m, 3H),

8.50-8.47 (br. s, 1H). HRMS (ESI) calcd for $C_{23}H_{31}ClN_3O_8S$: $[M-]^+$: 544.1526 Found 544.1537.

(B) White solid, mp 103–104°C, yield (70%),^{1}H NMR (400 MHz, *DMSO-d6*) δ ppm 0.92-0.85 (d, 6H), 1.74-1.43 (m, 4H), 2.28-2.02 (m, 2H), 2.98-2.81 (m, 3H), 3.85-3.72 (m, 4H), 3.99-3.95 (m, 2H), 4.32-4.06 (m, 2H), 5.01-4.79 (m, 2H), 7.36 (d, 1H), 7.75-7.63 (m, 3H), 8.52-8.49 (br. s, 1H). HRMS (ESI) calcd for $C_{23}H_{31}ClN_3O_8S$: $[M-]^+$: 544.1526 Found 544.1529.

Sodium (2S)-2-{(2S)-2-[5-(3-chlorobenzyl)-2-oxooxazolidin-3-yl]-3-cyclohexylpropanamido}-1-hydroxy-3-[(S)-2-oxopyrrolidin-3-yl] propane-1-sulfonate (13): White solid, yield (67%), mp 123–124°C, ^{1}H NMR (400 MHz, *DMSO-d6*) δ ppm 1.29-0.96 (m, 4H), 1.79-1.46 (m, 5H), 2.29-2.05 (m, 5H), 3.17-2.90 (m, 2H), 3.78-3.66 (m, 3H), 4.35-4.27 (m, 1H), 4.96-4.82 (br. s, 1H), 5.67-5.56 (m, 1H), 7.35 (d, J = 10.46 Hz, 1H), 7.66-7.63 (m, 3H), 8.47-8.40 (br. s, 1H). HRMS (ESI) calcd for $C_{26}H_{35}ClN_3O_8S$: $[M-]^+$: 584.1839 Found 584.1858.

Sodium (2S)-2-[(2S)-2-{5-[(3-chlorophenoxy)methyl]-2-oxooxazolidin-3-yl}-4-methylpentanamido]-1-hydroxy-3-[(S)-2-oxopyrrolidin-3-yl] propane-1-sulfonate (14): White solid, yield (68%), mp 69–70°C, ^{1}H NMR (400 MHz, *DMSO-d6*) δ ppm 0.92-0.82 (d, 6H), 1.21-1.02 (m, 1H), 2.36-1.88 (m, 7H), 3.21-2.94 (m, 5H), 4.06-3.64 (m, 2H), 4.55-4.10 (m, 2H), 5.06-4.86 (m, 2H), 7.03 (d, J = 9.48 Hz, 1H), 7.34-7.22 (m, 1H), 7.73-7.60 (m, 2H), 9.52-9.47 (br. s, 1H). HRMS (ESI) calcd for $C_{23}H_{31}ClN_3O_9S$: $[M-]^+$: 560.1475 Found 560.1502.

Sodium (2S)-2-[(2S)-2-(5-{[(3-chlorobenzyl)oxy]methyl}-2-oxooxazolidin-3-yl)-4-methylpentanamido]-1-hydroxy-3-[(S)-2-oxopyrrolidin-3-yl]propane-1-sulfonate (15): White solid, mp 40–41°C, yield (67%),^{1}H NMR (400 MHz, *DMSO-d6* δ 0.90-0.81 (dd, J = 18.13, 7.78 Hz, 6H), 1.71-1.40 (m, 1H), 2.21-2.00 (m, 6H), 3.20-2.90 (m, 2H), 3.64-3.54 (m, 3H), 3.78-3.64 (m, 2H), 4.55 (m, 1H), 4.85-4.75 (s, 2H), 7.39 (m, 2H), 7.71-7.63 (m, 2H), 8.51-8.46 (m, 1H). HRMS (ESI) calcd for $C_{24}H_{33}ClN_3O_9S$: $[M-]^+$: 574.1632 Found 574.1658.

4.2 X-ray crystallographic studies. Crystallization and data collection

Purified norovirus 3CL protease (NV 3CLpro) (10 mg/mL) in 100 mM NaCl, 50 mM PBS buffer, pH 7.2, and 1 mM dithiothreitol (DTT) was used for the preparation of the enzyme: ***8B*** complex. A stock solution of 100 mM inhibitor ***8B*** was prepared in DMSO and the NV 3CLpro:inhibitor complex was prepared by mixing 7 μL of inhibitor ***8B*** (3mM) with 243 μL (0.49 mM) of NV 3CLpro and incubating on ice for 1 h. The buffer was exchanged with 100 mM NaCl, 20 mM Tris pH 8.0 using a Zeba spin desalting column (MWCO=7 kDa, Life Technologies) and the sample was concentrated to 11.0 mg/mL for crystallization screening. All crystallization experiments were conducted with Compact Jr. (Rigaku Reagents) sitting drop vapor diffusion plates at 20 °C using equal volumes of protein and crystallization solution equilibrated against 75 μL of the latter. Crystals that displayed a prismatic morphology were obtained in 2–3 days from the Index HT screen (Hampton Research)

condition G2 (25% (w/v) polyethylene glycol 3350, 100 bis-Tris pH 5.5, 200 mM Li_2SO_4). Samples were transferred to a fresh drop composed of 80% crystallization solution and 20% (v/v) PEG 200 and stored in liquid nitrogen. X-ray diffraction data were collected at the Advanced Photon Source beamline 17-ID using a Dectris Pilatus 6M pixel array detector.

4.2.1 Structure Solution and Refinement—Intensities were integrated using XDS [41-k42] via Autoproc [43] and the Laue class analysis and data scaling were performed with Aimless [44]. Structure solution was conducted by molecular replacement with Phaser [45] using a previously determined isomorphous structure of inhibitor bound NV 3CLpro (PDB: 5T6D) [39] as the search model. Structure refinement and manual model building were conducted with Phenix [46] and Coot [47], respectively. Disordered side chains were truncated to the point for which electron density could be observed. Structure validation was conducted with Molprobity [48] and figures were prepared using the CCP4MG package [49].

4.3 FRET protease assays

The FRET protease assay was performed by preparing stock solutions of the substrate (Edans-DFHLQ/GP-Dabcyl) and inhibitor in DMSO and diluting into assay buffer which was comprised of 20 mM HEPES buffer, pH 8, containing NaCl (200 mM), 0.4 mM EDTA, glycerol (60%), and 6 mM dithiothreitol (DTT). The protease was mixed with serial dilutions of each compound up to 100 μM or with DMSO in 25 μL of assay buffer and incubated at 37 °C for 30 min, followed by the addition of 25 μL of assay buffer containing substrate. Fluorescence readings were obtained using an excitation wavelength of 360 nm and an emission wavelength of 460 nm on a fluorescence microplate reader (FLx800; Biotec, Winoosk, VT) for 1 h following the addition of substrate. Relative fluorescence units (RFU) were determined by subtracting background values (substrate-containing well without protease) from the raw fluorescence values, as described previously [31–36]. The dose-dependent FRET inhibition curves were fitted with a variable slope using GraphPad Prism software (GraphPad, La Jolla, CA) in order to determine the IC_{50} values of the inhibitors.

4.4 Cell-based inhibition assays

The effects of each inhibitor on virus replication were examined against NV in the NV replicon harboring cells (HG23 cells) [31]. Briefly, confluent and semi-confluent cells were incubated with medium containing DMSO (<0.1%) or each compound (up to 100 μM) for 48 h. After the incubation, total RNA was extracted and viral genome was quantitated with real-time quantitative RT-PCR (qRT-PCR). The EC_{50} values were determined by GraphPadPrism software [31].

4.5 Nonspecific cytotoxic effects

The cytotoxic dose for 50% cell death (CC_{50}) for each compound was determined for HG23 cells. Confluent cells grown in 96-well plates were treated with various concentrations (1–100 μM) of each compound for 72 h. Cell cytotoxicity was measured using a CytoTox 96 nonradioactive cytotoxicity assay kit (Promega, Madison, WI) and crystal violet staining. The in vitro therapeutic index was calculated by dividing the CC_{50} by the EC_{50}.

Supplementary Material

Refer to Web version on PubMed Central for supplementary material.

Acknowledgments

The generous financial support of this work by the National Institutes of Health (AI109039) is gratefully acknowledged. Use of the University of Kansas Protein Structure Laboratory was supported by a grant from the National Institute of General Medical Sciences (P30GM110761) of the National Institutes of Health. Use of the IMCA-CAT beamline 17-ID at the Advanced Photon Source was supported by the companies of the Industrial Macromolecular Crystallography Association through a contract with Hauptman-Woodward Medical Research Institute. Use of the Advanced Photon Source was supported by the U.S. Department of Energy, Office of Science, Office of Basic Energy Sciences under contract no. DE-AC02-06CH11357.

ABBREVIATIONS USED

PK	pharmacokinetics
DMF	N,N-dimethyl formamide
DCM	dichloromethane
CDI	carbonyl diimidazole
TLC	thin layer chromatography
EDCI	1-ethyl-3-(3-dimethylaminopropyl)carbodiimide
HOBt	N-hydroxybenzotriazole
DIEA	diisopropylethylamine
DTT	dithiothreitol
DMSO	dimethyl sulfoxide
IC_{50}	50% inhibitory concentration in the enzyme assay
EC_{50}	50% effective concentration in cell culture
CC_{50}	50% cytotoxic concentration in cell-based assays
GESAMT	general efficient structural alignment of macromolecular targets
rmsd	root mean-square deviation
XDS	X-ray detector software
ESI	electron spray ionization
RFU	relative fluorescence units

References

1. Koo HL, Ajami N, Atmar RL, DuPont HL. Noroviruses: the leading cause of gastroenteritis worldwide. Discov Med. 2010; 10:61–70. [PubMed: 20670600]

2. Bartsch SM, Lopman BA, Ozawa S, Hall AJ, Lee BY. Global economic burden of norovirus gastroenteritis. PLoS One. 2016; 11(4):e0151219. [PubMed: 27115736]
3. Lopman BA, Steele D, Kirkwood CD, Parashar UD. The vast and varied global burden of norovirus: prospects for prevention and control. PLoS Medicine. 2016; 13:e:1001999. [PubMed: 27115709]
4. Bok K, Green KY. Norovirus gastroenteritis in immunocompromised patients. New Engl J Med. 2012; 367:2126–2132. [PubMed: 23190223]
5. Hall AJ, Lopman BA, Payne DC, Patel MM, Gastanaduy PA, Vinje J, Parashar UD. Norovirus disease in the United States. Emerg Infect Dis. 2013; 19:1198–1205. [PubMed: 23876403]
6. Center for Disease Control and Prevention/Norovirus/Prevent the spread of Norovirus. [access on June 5, 2017] https://www.cdc.gov/features/norovirus/index.html
7. Robilotti E, Deresinski S, Pinsky BA. Noroviruses. Clin Microbiol Rev. 2015; 28:134–164. [PubMed: 25567225]
8. Lanata CF, Fischer-Walker CL, Olascoaga AC, Torres CX, Aryee MKJ, Black RE. Global causes of diarrheal disease mortality in children <5 years of age: a systematic review. PLoS One. 2013; 8:e72788. [PubMed: 24023773]
9. Kim Y, Galasiti Kankanamalage AC, Chang K-O, Groutas WC. Recent advances in the discovery of norovirus therapeutics. J Med Chem. 2015; 58:9438–9450. [PubMed: 26258852]
10. Galasiti Kankanamalage AC, Weerawarna PM, Kim Y, Chang K-O, Groutas WC. Anti-norovirus therapeutics: a patent review (2010–2015). Expert Opin Ther Pat. 2016; 26:297–308. [PubMed: 26881878]
11. Venkataraman Prasad BV, Shanker S, Muhaxhiri Z, Deng L, Choi J-M, Estes MK, Song Y, Palzkill T, Atmar RL. Antiviral targets of human noroviruses. Curr Opin Virol. 2016; 18:117–125. [PubMed: 27318434]
12. Weerasekara S, Prior AM, Hua DH. Current tools for norovirus drug discovery. Expert Opin Drug Discov. 2016; 11:529–541. [PubMed: 27108716]
13. Kocher J, Yuan L. Norovirus vaccines and potential anti-norovirus drugs: recent advances and future perspectives. Future Virol. 2015; 10:899–913. [PubMed: 26568768]
14. Rocha-Pereira J, Neyts J, Jochmans D. Norovirus: targets and tools in antiviral drug discovery. Biochem Pharmacol. 2014; 91:1–11. [PubMed: 24893351]
15. Karst SM, Tibbetts SA. Recent advances in understanding norovirus pathogenesis. J Med Virol. 2016; 88:1837–1843. [PubMed: 27110852]
16. Bartnicki E, Cunha JB, Kolawole AO, Wobus CE. Recent advances in understanding noroviruses. F1000Research. 2017; 6:79-. [PubMed: 28163914]
17. Karst SM, Wobus CE. A working model of how noroviruses infect the intestine. PLoS Pathogens. 2015; 11:e:1004626. [PubMed: 25723501]
18. Orchard RC, Wilen CB, Doench JG, Baldridge MT, McCune BT, Lee Y-CJ, Lee S, Pruett-Miller SM, Nelson CA, Fremont DH, Virgin HW. Discovery of a proteinaceous cellular receptor for a norovirus. 2016; 353:933–936.
19. Haga K, Fujimoto A, Yakai-Todaka R, Miki M, Doan YH, Murakami K, Yokoyama M, Murata K, Nakanishi A, Katayama K. Functional receptor molecules CD300lf and CD300ld within the CD300 family enable murine noroviruses to infect cells. Proc Natl Acad Sci USA. 2016; 113:E6248–E6255. [PubMed: 27681626]
20. Karst SM. The influence of commensal bacteria on infection with enteric viruses. Nat Rev Microbiol. 2016; 14:197–204. [PubMed: 26853118]
21. Karst SM. Identification of a novel cellular target and a co-factor for norovirus infection – B cells and commensal bacteria. Gut Microbes. 2015; 6:266–271. [PubMed: 25997033]
22. Yu H, Hasan NM, In JG, Estes MK, Kovbasnjuk O, Zachos NC, Donowitz M. The contributions of human mini-intestines to the study of intestinal physiology and pathophysiology. Annu Rev Physiol. 2017; 79:291–312. [PubMed: 28192061]
23. Taube S, Kolawole AO, Hohne M, Wilkinson JE, Handley SA, Perry JW, Thackray LB, Akkina R, Wobus CE. A mouse model for human norovirus. MBio. 2013; 4:e00450–13. [PubMed: 23860770]

24. Kim, KY. Caliciviridae: The Noroviruses. In: Knipe, DM., editor. Field's Virology. 6. Vol. 1. Lippincott Williams & Wilkins; Philadelphia, PA: 2013. p. 582-608.
25. Thorne LG, Goodfellow IG. Norovirus gene expression and replication. J Gen Virol. 2014; 95:278–291. [PubMed: 24243731]
26. Karst SM, Wobus CE, Goodfellow IG, Green KY, Virgin HW. Advances in norovirus biology. Cell Host Microbe. 2014; 15:668–680. [PubMed: 24922570]
27. Hussey RJ, Coates L, Gill RS, Erskine PT, Coker SF, Mitchell E, Cooper JB, Broadbridge R, Clarke IN, Lambden PR, Shoolingin-Jordan PM. Structural study of norovirus 3C specificity: binding of a designed active site-directed peptide inhibitor. Biochemistry. 2011; 50:240–249. [PubMed: 21128685]
28. Hardy ME, Crone TJ, Brower JE, Ettayebi K. Substrate specificity of the Norwalk virus 3C-like proteinase. Virus Res. 2002; 89:29–39. [PubMed: 12367748]
29. Muhaxhiri Z, Deng L, Shanker S, Sankaran B, Estes MK, Palzkill T, Song Y, Venkataram Prasad BV. Structural basis of substrate specificity and protease inhibition in Norwalk virus. J Virol. 2013; 87:4281–4292. [PubMed: 23365454]
30. Nomenclature used is that of L. Schechter. A Berger, Biochem Biophys Res Comm. 1967; 27:157–162. where S_1, S_2, S_3, …. S_n and S_1', S_2', S_3', …. S_n' correspond to the enzyme subsites on the N-terminus and C-terminus side, respectively, of the scissile bond. Each subsite accommodates a corresponding amino acid residue side chain designated P_1, P_2, P_3,…..P_n and P_1', P_2', P_3',…..P_n' of a substrate or inhibitor. P_1 is the primary substrate specificity residue and P_1-P_1' is the scissile bond. [PubMed: 6035483]
31. Galasiti Kankanamalage AC, Kim Y, Weerawarna PM, Uy RA, Damalanka VC, Mandadapu SR, Alliston KR, Mehzabeen N, Battaille KP, Lovell S, Chang K-O, Groutas WC. Structure-guided design and optimization of norovirus 3CL protease. Structure-activity relationships and biochemical, X-ray crystallographic, cell-based and in vivo studies. J Med Chem. 2015; 58:3144–3155. [PubMed: 25761614]
32. Damalanka VC, Kim Y, Alliston KR, Weerawarna PM, Galasiti Kankanamalage AC, Lushington GH, Mehzabeen N, Battaille KP, Lovell S, Chang K-O, Groutas WC. Oxadiazole-based cell permeable macrocyclic transition state inhibitors of norovirus 3CL protease. J Med Chem. 2016; 59:1899–1913. [PubMed: 26823007]
33. Weerawarna PM, Kim Y, Galasiti Kankanamalage AC, Damalanka VC, Lushington GH, Alliston KR, Mehzabeen N, Battaille KP, Lovell S, Chang K-O, Groutas WC. Structure-based design and synthesis of triazole-based macrocyclic inhibitors of norovirus protease: structural, biochemical, spectroscopic, and antiviral studies. Eur J Med Chem. 2016; 119:300–318. [PubMed: 27235842]
34. Kim Y, Lovell S, Tiew KC, Mandadapu SR, Alliston KR, Battaille KP, Groutas WC, Chang KO. Broad-spectrum antivirals against 3CL or 3C-like proteases of picornaviruses. noroviruses and coronaviruses. J Virol. 2012; 6:1754–1762.
35. Galasiti Kankanamalage AC, Kim Y, Rathnayake AD, Alliston KR, Butler MM, Cardinale SC, Bowlin TL, Groutas WC, Chang CO. Design, synthesis and evaluation of novel prodrugs of transition state inhibitors of norovirus 3CL protease. J Med Chem. 2017; 60:6239–6248. [PubMed: 28671827]
36. Damalanka VC, Kim Y, Galasiti Kankanamalage AC, Lushington GH, Mehzabeen N, Battaille KP, Lovell S, Chang KO, Groutas WC. Design, synthesis and evaluation of a novel series of macrocyclic inhibotors of norovirus 3CL protease. Eur J Med Chem. 2017; 127:41–61. [PubMed: 28038326]
37. Deng L, Muhaxhiri Z, Estes MK, Palzkill T, Venkataram Prasad BV, Song Y. Synthesis, activity, and structure-activity relationship of noroviral protease inhibitors. MedChemComm. 2013; 4:1354–1359.
38. Webster SE, Okano K, Little TL, Reich SH, Xin Y, Fuhrman SA, Matthews DA, Love RA, Hendrickson TF, Patick AK, Meador JW, Ferre RA, Brown EL, Ford CE, Binford SL, Worland ST. Tripeptide aldehyde inhibitors of human rhinovirus 3C protease: design, synthesis, biological evaluation, and cocrystal structure solution of P1 glutamine isosteric replacements. J Med Chem. 1998; 41:2786–2805. [PubMed: 9667969]
39. Galasiti Kankanamalage AC, Kim Y, Rathnayake AD, Damalanka VC, Weerawarna PM, Doyle ST, Alsoudi AF, Padmasankha Dissayanake DM, Lushington GH, Mehzabeen N, Battaille KP, Lovell

S, Chang KO, Groutas WC. Structure-based exploration and exploitation of the S_4 subsite of norovirus 3CL protease in the design of potent and permeable inhibitors. Eur J Med Chem. 2017; 126:502–516. [PubMed: 27914364]

40. Krissinel E. Enhanced fold recognition using efficient short fragment clustering. J Mol Biochem. 2012; 1:76–85. [PubMed: 27882309]
41. Kabsch W. Automatic Indexing of Rotation Diffraction Patterns. J Appl Crystallogr. 1988; 21:67–72.
42. Kabsch W. Xds Acta Crystallogr D Biol Crystallogr. 2010; 66:125–132. [PubMed: 20124692]
43. Vonrhein C, Flensburg C, Keller P, Sharff A, Smart O, Paciorek W, Womack T, Bricogne G. Data processing and analysis with the autoPROC toolbox. Acta Crystallogr D Biol Crystallogr. 2011; 67(Pt4):293–302. [PubMed: 21460447]
44. Evans PR. An introduction to data reduction: space-group determination, scaling and intensity statistics. Acta Crystallogr D Biol Crystallogr. 2011; 67:282–292. [PubMed: 21460446]
45. McCoy AJ, Grosse-Kunstleve RW, Adams PD, Winn M, Storoni LC, Read RJ. Phaser crystallographic software. J Appl Cryst. 2007; 40:658–674. [PubMed: 19461840]
46. Adams PD, Afonine PV, Bunkoczi G, Chen VB, David IW, Echols N, Headd JJ, Hung LW, Kapral GJ, Grosse-Kunstleve RW, McCoy AJ, Moriarty NW, Oeffner R, Read RJ, Richardson DC, Richardson JS, Terwilliger TC, Zwart PH. PHENIX: a comprehensive python-based system for macromolecular structure solution. Acta Crystallogr Sect D: Biol Crystallogr. 2010; 66:213–221. [PubMed: 20124702]
47. Emsley P, Lohkamp B, Scott WG, Cowtan K. Features and development of Coot. Acta Crystallogr Sect D: Biol Crystallogr. 2010; 66:486–501. [PubMed: 20383002]
48. Chen VB, Arendall WB, Headd JJ, Keedy DA, Immormino RM, Kapral GJ, Murray LW, Richardson JS, Richardson DC. MolProbity: All-atom structure validation for macromolecular crystallography. Acta Crystallogr Sect D: Biol Crystallogr. 2010; 66:12–21. [PubMed: 20057044]
49. Potterton L, McNicholas S, Krissinel E, Gruber J, Cowlan K, Emlsey P, Murshudov GN, Cohen S, Perrakis A, Noble M. Developments in the CCP4 molecular graphics project. Acta Crystallogr Sect D: Biol Crystallogr. 2004; 60:2288–2294. [PubMed: 15572783]
50. Evans P. Scaling and assessment of data quality. Acta Crystallogr Sect D: Biol Crystallogr. 2006; 62:72–82. [PubMed: 16369096]
51. Diederichs K, Karplus PA. Improved R-factors for diffraction data analysis in macromolecular crystallography. Nat Struct Biol. 1997; 4:269–275. [PubMed: 9095194]
52. Weiss MS. Global indicators of X-ray data quality. J Appl Crystallogr. 2001; 34:130–135.
53. Karplus PA, Diederichs K. Linking crystallographic model and data quality. Science. 2012; 336:1030–1033. [PubMed: 22628654]
54. Evans P. Biochemistry. Resolving some old problems in protein crystallography. Science. 2012; 336:986–987. [PubMed: 22628641]
55. Afonine PV, Grosse-Kunstleve RW, Echols N, Headd JJ, Moriarty NW, Mustyakimov N, Terwilliger TC, Urzhumtsev A, Zwart PH, Adams PD. Towards automated crystallographic structure refinement with phenix. refine. Acta Crystallogr. 2012; 60:352–367.

Appendix A. Supplementary data

Supplementary data related to this article can be found at …….

- The structure-guided design of a series of novel oxazolidinone-based inhibitors of norovirus 3CL protease inhibitors is reported.
- Cell-permeable low micromolar inhibitors have been identified.
- The mechanism of action and mode of binding of the inhibitors were unraveled using X-ray crystallography.
- The interaction of the inhibitors with the enzyme is associated with structural rearrangements that impact pharmacological activity.

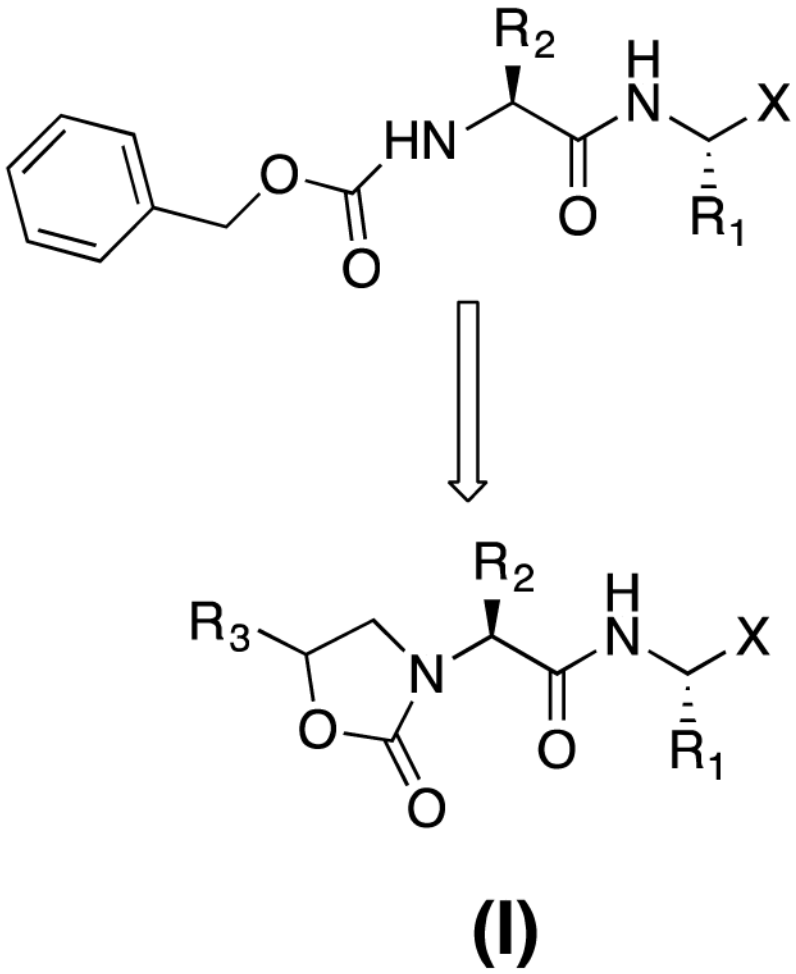

Fig. 1.
Design and general structure of inhibitor (I)

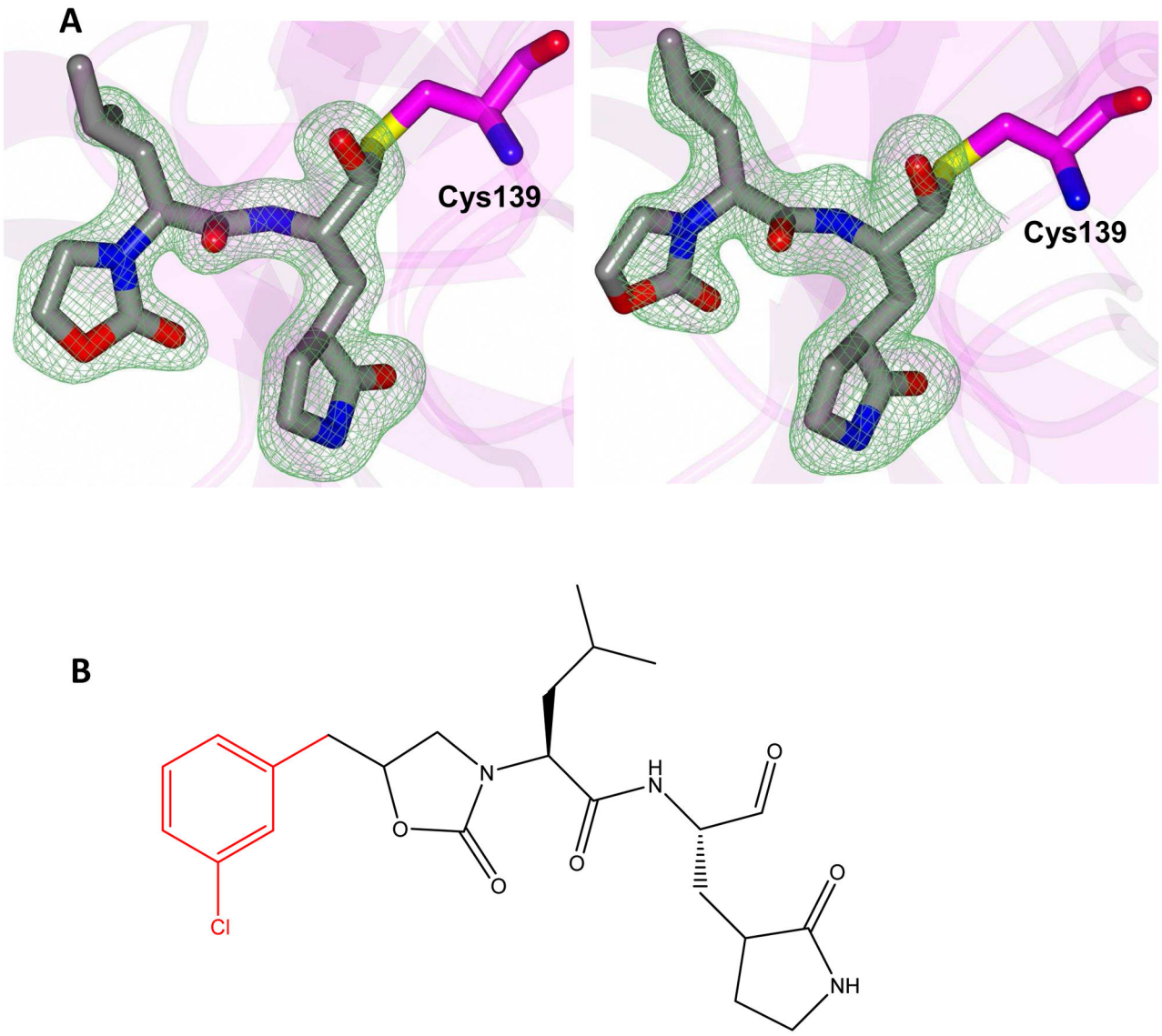

Figure 2.

A) Fo-Fc polder omit map [53] of inhibitor ***8B*** (green mesh) contoured at 3σ. The ligand associated with subunits A and B is positioned on the left and right, respectively. **B)** Structure of inhibitor ***8B*** with the disordered m-chlorobenzyl group highlighted in red.

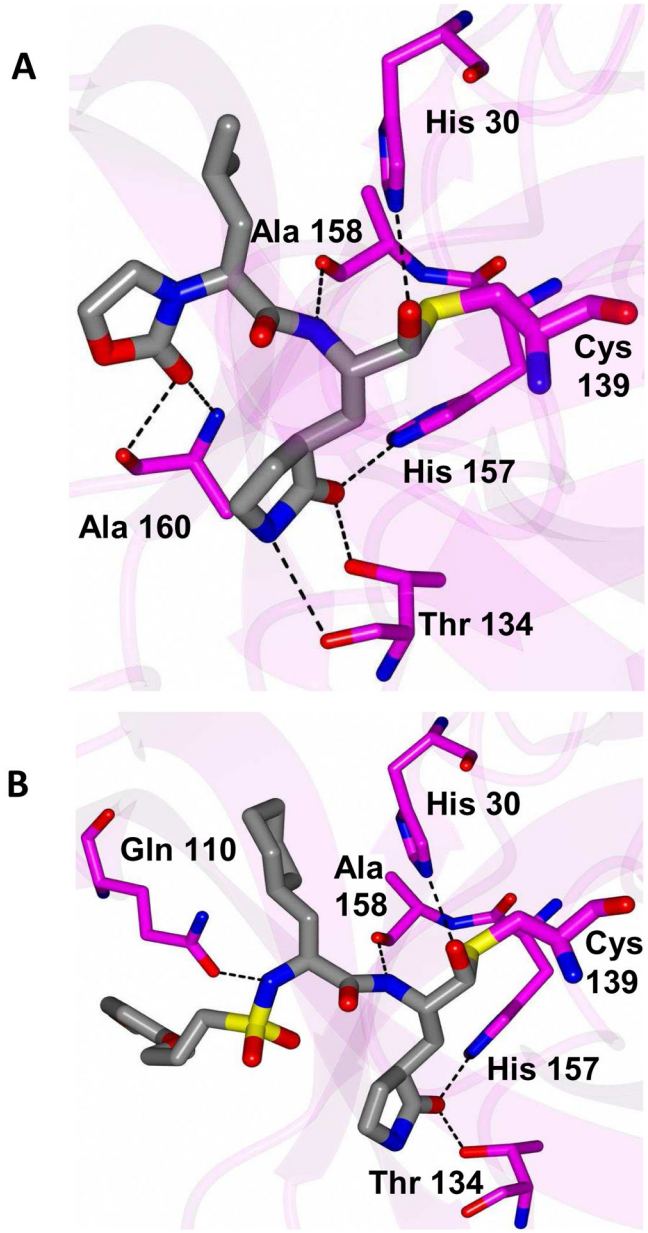

Figure 3.

Hydrogen bond interactions (dashed lines) for NV 3CLpro in complex with **A)** compound ***8B*** and **B)** *5T6D* [39].

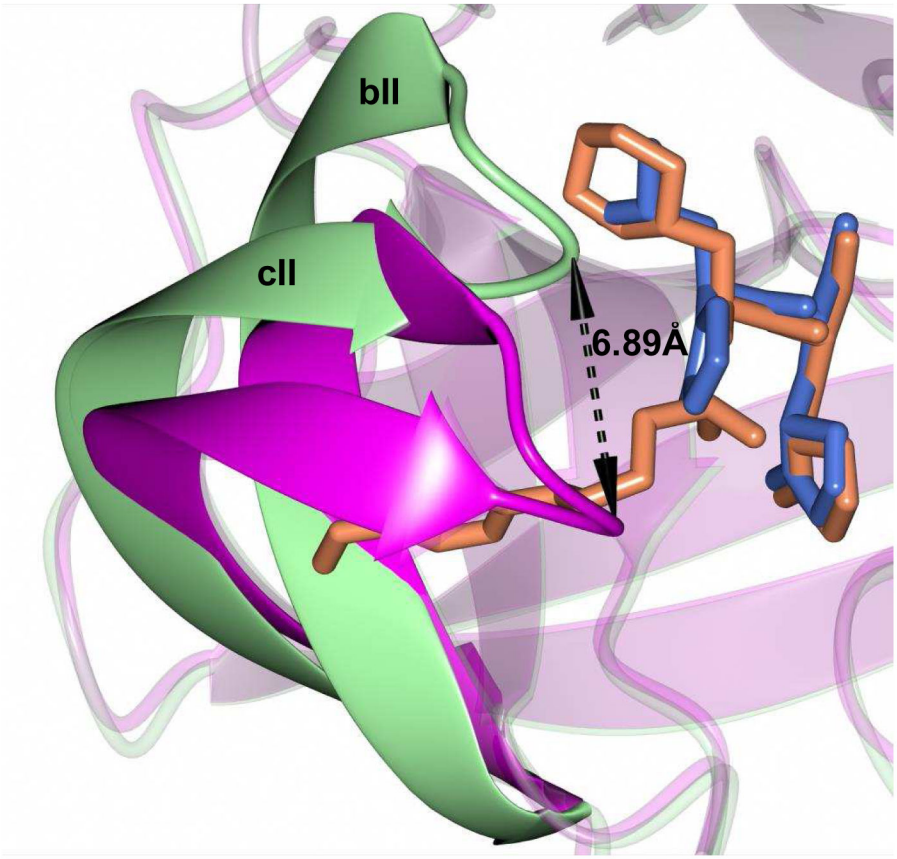

Figure 4.

Superposition of NV 3CLpro:***8B*** (magenta) with ***5T6D*** (green). The inhibitors are colored blue and tan for each respective structure. The arrow indicates the positions of Gln 110 for each structure.

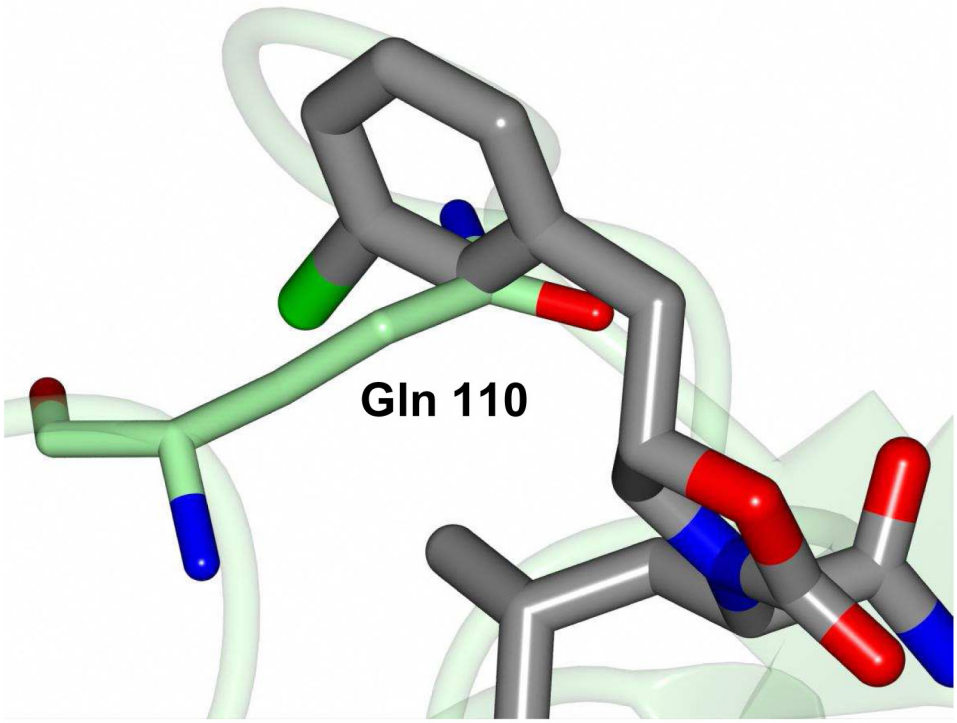

Figure 5.

Inclusion of the *m*-chorobenzyl ring of inhibitor ***8B*** in an idealized position superimposed onto the 5T6D structure (green). The aryl ring occupies the same space and Gln 110 and results in the observed conformational change shown in Figure 4.

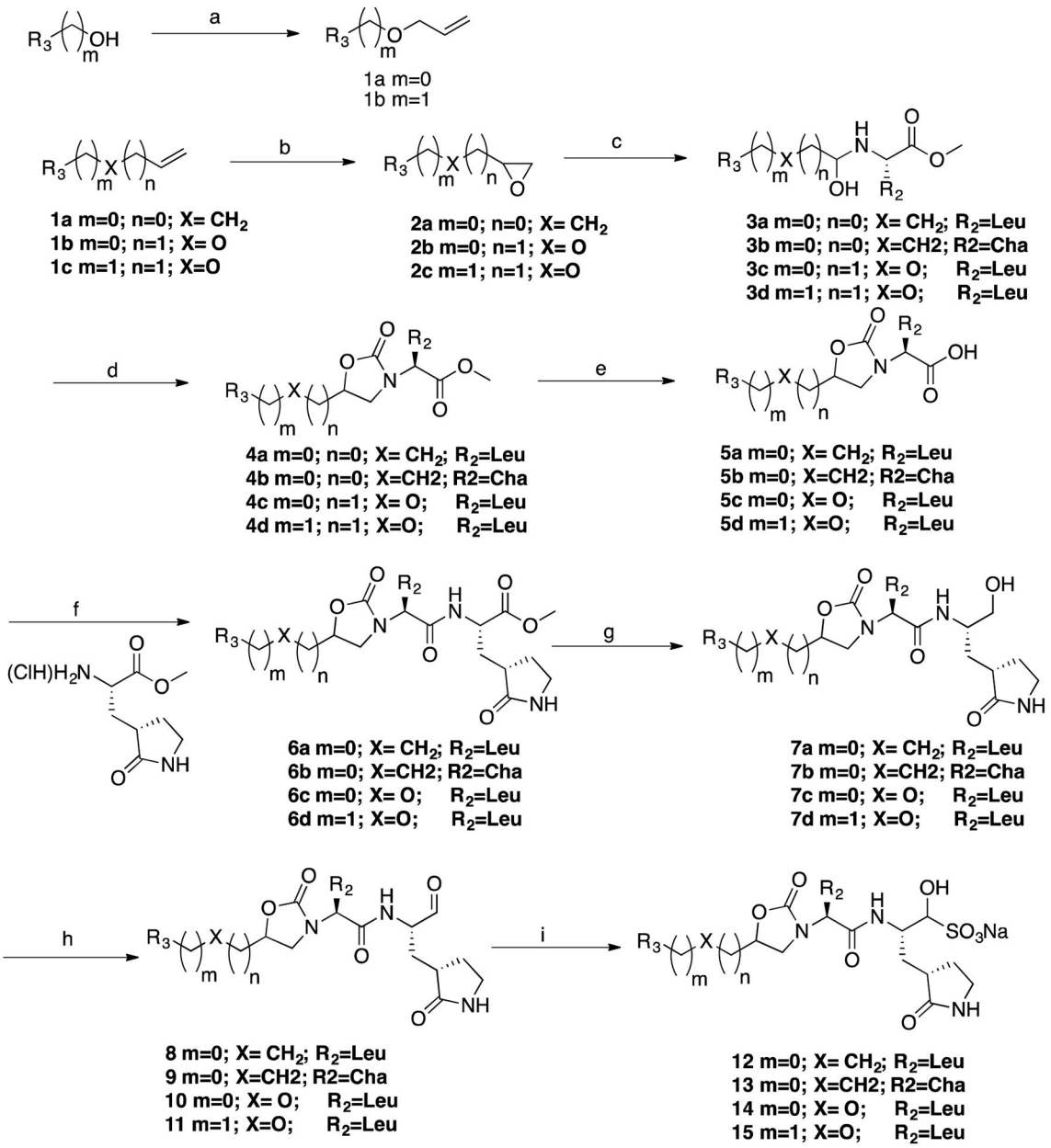

Scheme 1.

a) NaH/allyl bromide/DMF; b) MCPBA/DCM; c) (L)Leu-OCH_3 or (L)Cha-OCH_3/TFE; d) CDI/THF; e) LiOH/aq.THF; f) EDCI/HOBt/DIEA/DMF; g) 2M $LiBH_4$/THF/CH_3OH; h) Dess-Martin periodinane/DCM; h) $NaHSO_3$/EtOAc/CH_3CH_2OH/H_2O

Table 1

Inhibitory activity of compounds ***8–15.***

Compound	R_3	R_2	X	IC_{50} (μM)	EC_{50} (μM)	CC_{50} (μM)
8A	*m*-Cl phenyl	Leu	CHO	7.3	11.5	> 100
12A			$CH(OH)SO_3Na$	8.2	12.3	> 100
8B	*m*-Cl phenyl	Leu	CHO	15.3	15.3	> 100
12B			$CH(OH)SO_3Na$	13.2	17.5	> 100
9[a]	*m*-Cl phenyl	Cha	CHO	13.5	6.7	55.2
13			$CH(OH)SO_3Na$	15.1	8.1	46.1
10[a]	*m*-Cl phenoxy methyl	Leu	CHO	3.8	8.2	> 100
14[a]			$CH(OH)SO_3Na$	8.5	7.6	> 100
11[a]	*m*-Cl benzyloxy methyl	Leu	CHO	8.1	14.8	> 100
15[a]			$CH(OH)SO_3Na$	10.6	17.3	> 100

[a]screened as mixtures of diastereomers

Table 2

Crystallographic data for norovirus 3CL protease in complex with inhibitor ***8B.***

	NVPro:*8B*
Data Collection	
Unit-cell parameters (Å, °)	$a=b$=59.56, c=357.55
Space group	$P6_122$
Resolution (Å)[a]	49.56-1.95 (2.00-1.95)
Wavelength (Å)	1.0000
Temperature (K)	100
Observed reflections	542,337
Unique reflections	29,026
<I/σ(I)>[a]	18.1 (2.2)
Completeness (%)[a]	100 (100)
Multiplicity[a]	18.7 (19.6)
R_{merge} (%)[a,b]	13.4 (182.5)
R_{meas} (%)[a,d]	13.8 (187.0)
R_{pim} (%)[a,d]	3.2 (41.7)
$CC_{1/2}$ [a,e]	0.999 (0.775)
Refinement	
Resolution (Å)[a]	36.29-1.95
Reflections (working/test)	27,471/1,400
R_{factor}/R_{free} (%)[c]	18.8/22.9
No. of atoms (Protein/Ligand/Water)	2,430/48/147
Model Quality	
R.m.s deviations	
Bond lengths (Å)	0.010
Bond angles (°)	1.020
Average *B*-factor (Å^2)	
All Atoms	35.1
Protein	34.7
Ligand	37.2
Water	41.5
Coordinate error(maximum likelihood) (Å)	0.18
Ramachandran Plot	
Most favored (%)	97.9
Additionally allowed (%)	2.1

[a] Values in parenthesis are for the highest resolution shell.

[b] $R_{merge} = \Sigma_{hkl}\Sigma_i |I_i(hkl) - \langle I(hkl)\rangle| / \Sigma_{hkl}\Sigma_i I_i(hkl)$, where $I_i(hkl)$ is the intensity measured for the ith reflection and $\langle I(hkl)\rangle$ is the average intensity of all reflections with indices hkl.

[c] $R_{factor} = \Sigma_{hkl} ||F_{obs}(hkl)| - |F_{calc}(hkl)|| / \Sigma_{hkl} |F_{obs}(hkl)|$; Rfree is calculated in an identical manner using 5% of randomly selected reflections that were not included in the refinement.

[d] R_{meas} = redundancy-independent (multiplicity-weighted) R_{merge}[50–51]. R_{pim} = precision-indicating (multiplicity-weighted) R_{merge}[52–53].

[e] $CC_{1/2}$ is the correlation coefficient of the mean intensities between two random half-sets of data [54–55].